Exploring the Electronic Structure of New Doped Salt Hydrates, $Mg_{1-x}Ca_xCl_2 \cdot nH_2O$, for Thermochemical Energy Storage

THE JOURNAL OF PHYSICAL CHEMISTRY C

pubs.acs.org/JPCC

Article

Exploring the Electronic Structure of New Doped Salt Hydrates, $Mg_{1-x}Ca_xCl_2{\cdot}nH_2O$, for Thermochemical Energy Storage

Koen Heijmans, Ionut C. Tranca,* Silvia V. Gaastra-Nedea,* and David M. J. Smeulders

Cite This: *J. Phys. Chem. C* 2020, 124, 24580–24591

Read Online

ACCESS | Metrics & More | Article Recommendations | Supporting Information

ABSTRACT: Chloride-based salt hydrates, $MgCl_2{\cdot}nH_2O$ and $CaCl_2{\cdot}nH_2O$ (n = 0,1,2,4,6), are promising materials for thermochemical heat storage systems due to their high sorption energy capacity. However, both salts have their own shortcoming characteristics within the operational temperature of the thermochemical heat storage applications. While the higher hydrates of $CaCl_2{\cdot}nH_2O$ (n = 4,6) have a low melting point, the lower hydrates of $MgCl_2{\cdot}nH_2O$ (n = 0,1,2) can form the highly toxic and corrosive HCl gas. Both shortcomings cap the individual use of these salts to a restricted range of the available hydrates. A combination of these two salts showed to have the potential to overcome these shortcomings. The present study focuses on finding stable configurations of potential superior salt hydrate combinations using the evolutionary algorithm USPEX as well as manual mutations of known pristine structures. The newly found structures are less stable than the pure salts, but stable enough to be combined. Extensive electronic density-derived tools, like the Density Derived Electronic and Chemical (DDEC6) bond orders and net atomic charges, as well as Bader topological analysis, are used to predict the HCl gas formation based on the chemical environment in the new metastable structures. We find that doping $MgCl_2{\cdot}nH_2O$ with calcium considerably reduces HCl formation compared to its pure form, caused by a combination of the stronger Ca−Cl interaction than Mg−Cl and a less polar H_2O molecule in a calcium environment than in a magnesium environment. This provides the possibility to shift the p, T-equilibrium curve of HCl outside the thermal storage operational window.

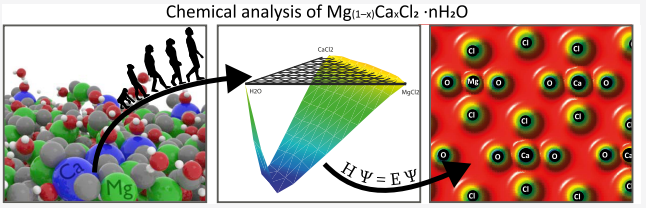

INTRODUCTION

In the transition toward a new energy society, based on renewable sources, a long-term energy storage is key to bridge the mismatch between solar irradiation and heat demand of different users. Such a system can make a major contribution, since hot tap water and space heating combined account for 79% of the final energy use of EU households.[1] Therefore, there is a growing interest in a storage system, which stores large amounts of heat, with negligible heat losses over long time periods, in a compact design. Thermochemical heat storage has the means to achieve this goal. It stores heat in a reversible reaction between a sorbate and a sorbent[2−4] according to the reaction

$$A + B \rightleftharpoons AB + Q$$

When there is an excess of heat, the sorbate (A) and the sorbent (B) are combined via an endothermic reaction to material AB, while heat (Q) is released. In times of abundant heat, heat is used to split the material AB, via an endothermic reaction, back to the original sorbate (A) and sorbent (B). Especially, thermochemical heat storage systems based on gas−solid sorption mechanisms have theoretical high energy storage capacities, compared to other heat storage system. These solid sorption systems can roughly be divided into two groups, weak chemisorption of vapors in salts (e.g., salt in combination with water, ammonia, ethanol, or methanol) and strong chemisorption (e.g., metallic hydrides, hydroxides, carbonates).[5] Strong chemisorption reactions form a strong bond between the sorbent and sorbate, which results in medium to high thermochemical storage operating temperatures. For example, hydrogen systems like metal hydride and hydroxide systems typically operate at medium temperatures ($523 < T < 723$ K) and carbonates at high temperatures ($T > 723$ K).[6] Accordingly, these systems are usually applied in industry. Weak chemisorption interactions lead to low operating temperatures ($T < 523$ K), which makes them ideal for domestic heating. Weak chemisorption systems make use of salt hydrates mostly in combination with water vapor, because of practical reasons like the abundance of water vapor in air. The reversible (de)hydration reaction of the salts can occur in multiple hydration steps, following: $salt{\cdot}nH_2O(s) + Q \rightleftharpoons salt{\cdot}(n-m)H_2O(s) + mH_2O(g)$.

When salt hydrates are heated, they dissociate in water vapor and a lower hydrate or anhydrous salt. When water is added to

Received: June 25, 2020
Revised: October 6, 2020
Published: October 29, 2020

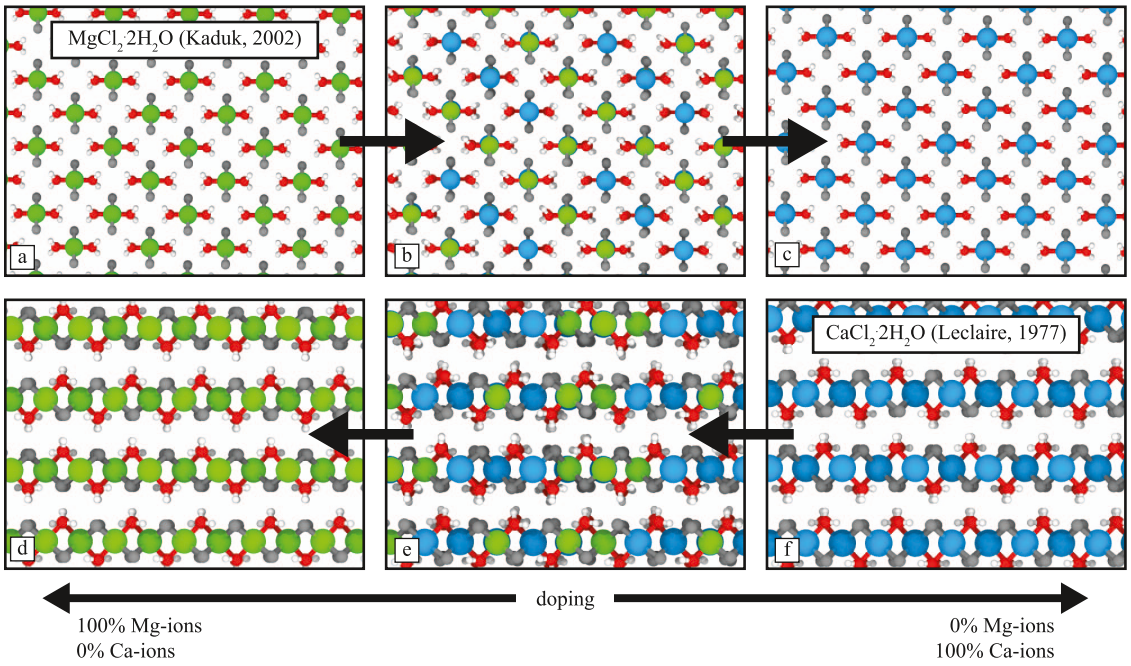

Figure 1. Schematic representation of the approach for manually creating the doped salt hydrates.[18] The example of the dihydrate salts, $MgCl_2 \cdot 2H_2O$ and $CaCl_2 \cdot 2H_2O$, is presented, with these two salts constituting both the starting and ending points.[33,34] The green spheres represent magnesium atoms; blue, calcium; gray, chlorides; red, oxygens; and light gray, hydrogens.

an anhydrous or lower hydrate salt, they combine to a higher hydrate, and heat is released. Ideal thermochemical materials (TCM) for such storage should have a high energy density, be affordable, have a high cycle stability, have fast kinetics, and should be nontoxic. In this sense, large amounts of different salts have been studied and reviewed.[2−5,7−9] A promising group of these TCM salt hydrates are chloride-based $MgCl_2 \cdot nH_2O$ and $CaCl_2 \cdot nH_2O$ (n = 0, 1, 2, 4, 6). The main reasons are the relatively high sorption energy (2−3 GJ/m^3), cost, and availability.[10] Furthermore, the reactions of these salts occur at temperatures corresponding to domestic heating applications.[11] Dehydration temperatures range from 36 to 214 °C, depending on the current hydration level. Thus, $MgCl_2 \cdot nH_2O$ dehydrates at temperatures of 214, 125−127, 101−104, and 68−72 °C, for n = 1, 2, 4, and 6 respectively, and $CaCl_2 \cdot nH_2O$ dehydrates at 36−41, 49−54, 71, and 112 °C, for n = 1, 2, 4, and 6 respectively.[7] In practice, mainly the hydration levels n = 2−6 for pristine $MgCl_2 \cdot nH_2O$ and n = 0−2 for pristine $CaCl_2 \cdot nH_2O$ are considered as TCM, due to different concerns when these pure salts are used. A point of concern is the deliquesce,[8] which occurs for both salts already at low temperatures (25 °C) if the water vapor pressure is sufficiently high enough (12 mbar).[7,12,13] Besides, in the case of calcium chloride, higher hydrates like $CaCl_2 \cdot 4H_2O$ and $CaCl_2 \cdot 6H_2O$ have low melting temperatures, which are in the range of the storage operation window.[14,15] Both phenomena, deliquesce and melting, can lead to agglomerates and clog the storage system. A major disadvantage of $MgCl_2$ hydrates is hydrolysis (formation of HCl) above 135 °C[11,16] ($MgCl_2 \cdot H_2O(s) \rightarrow MgOHCl(s) + HCl(g)$).

This is an undesired irreversible reaction, which degrades the storage materials, and most importantly, HCl is a highly toxic and corrosive gas. These shortcomings of $MgCl_2$ and $CaCl_2$ salts cap the use of the entire range of the hydrates and make them less convenient to be used as TCM.

$CaCl_2 \cdot H_2O$ is more resistant to hydrolysis than $MgCl_2 \cdot H_2O$.[17] On the other hand, $MgCl_2 \cdot 6H_2O$ has a higher melting point than $CaCl_2 \cdot 6H_2O$ and remains solid within the storage operation window. This implies that a potential combination of $CaCl_2 \cdot nH_2O$ and $MgCl_2 \cdot nH_2O$ could have superior characteristics compared to their isolated pure components, regarding increased stability and reduced hydrolysis. This assumption is supported by multiple studies.[18−22] Rammelberg et al.[19,20] experimentally showed an improved cyclability for a mixture of $MgCl_2/CaCl_2$. Pathak et al.[21] found, using density functional theory (DFT), that a double salt of $CaCl_2$ and $MgCl_2$ is more resistant to hydrolysis than the individual pure compounds. Furthermore, diffusion of water through the salt crystals is typically very slow,[10,23] limiting the applicability of these salts as TCM. Imperfections in the crystal, e.g., stresses created by defects, boundaries, impurities, and interfaces, could promote the diffusion of water.[23−25] Müller et al.[22] experimentally observed for a similar system of magnesium oxides, doped with 0−40% calcium, a significantly increased water dissociation rate. This doping enhances the hydration rate as well as the cycle stability, with the optimum value being found for 10% doping. They supported their experimental findings with DFT calculations, which indicated that the calcium dopant expanded the surface lattice of MgO toward the CaO surface and it increased water dissociation.

Huinink et al.[23] showed that for bulk $MgCl_2 \cdot 4H_2O$ and $MgCl_2 \cdot 6H_2O$, an interstitial water molecule diffuses faster than the water molecules fixed in the coordination shells of the magnesium ion. In addition, they concluded that a substituted calcium atom into a bulk magnesium crystal can absorb and pin the interstitial water molecule, limiting its mobility. However, Huinink et al. focused on bulk material, where the diffusion can be orders of magnitude lower than in regions close to the surface,[24,25] which is the region Müller et al. did their findings. The surface characteristics play an important role in many saltlike structures, as low reactivity and cycle

https://dx.doi.org/10.1021/acs.jpcc.0c05799
J. Phys. Chem. C 2020, 124, 24580−24591

stability are correlated to the critical inhibition of water near the surface,[22,26] and an increased lattice at the surface promotes water dissociation. This increased water dissociation could improve water dehydration and transport, which are important design parameters for heat storage systems.[8,27] As listed before, the different dehydration temperatures do not exactly match between the pure salts. In this sense, new/intermediate dehydration temperatures could be expected when the salts are combined. Alternatively, different dehydration onset temperatures could act as nucleation sites in the combination of the salts.

Based on these previous studies, $MgCl_2$ doped with calcium could improve key material properties for thermochemical storage. The AFLOW-CHULL platform[28] computed the convex hull for ternary combinations of Ca, Mg, and Cl. They found as the only stable structures: pure Ca, pure Mg, pure Cl, $CaCl_2$, $MgCl_2$, and $CaMg_2$. In the present work, we extended the search and focused on the combinations of $MgCl_2{\cdot}nH_2O$ and $CaCl_2{\cdot}nH_2O$, because of the heat storage application. In this sense, we used the evolutionary algorithm USPEX,[29−31] as well as manually doped crystals, to predict new structures of $Mg_xCa_{(1-x)}Cl_2{\cdot}nH_2O$ (n = 0, 2, 4, 6; x = [0, 1]). Afterward, using first-principles analysis tools, the chemical effect of doping on the stability of the crystals, hydrolysis, and the volumetric energy density of the storage material were investigated.

METHODS

Exploration of New Doped Structures. Two methods were used to explore new possible combinations of $MgCl_2{\cdot}nH_2O$ and $CaCl_2{\cdot}nH_2O$, manually doping the structures and automatic structure generation using the evolutionary algorithm USPEX. The stability of these new combinations was analyzed using the convex hull method.

Manually Doped Structures. Manually doped structures were created for all of the hydrates. We started from the experimentally known salt hydrate structures $MgCl_2$,[32] $CaCl_2$,[32] $MgCl_2{\cdot}2H_2O$,[33] $CaCl_2{\cdot}2H_2O$,[34] $MgCl_2{\cdot}4\ H_2O$,[35] $CaCl_2{\cdot}4H_2O$,[36] $MgCl_2{\cdot}6H_2O$,[37] and $CaCl_2{\cdot}6H_2O$.[38] In these known structures, Mg atoms were gradually substituted by Ca atoms and vice versa (Mg ↔ Ca), as shown in Figure 1. This resulted in numerous $Mg_{(1-x)}Ca_xCl_2{\cdot}nH_2O$ crystals, with x = [0, 1] and n = 0, 2, 4, and 6. The generated structures were relaxed using the DFT Vienna Ab initio Simulation Package (VASP).[39] The Perdew−Burke−Ernzerhof (PBE)[40] exchange−correlation functions, with the projector-augmented wave (PAW)[41,42] scheme, were used to describe the ion−electron interactions. The DFT-D3,[43] including the Becke−Johnson damping,[44] was used to describe the dispersion interactions. Each generated structure was relaxed until all forces on the atoms were lower than 0.026 eV/Å. Accordingly, the structure stabilities were analyzed by computing the convex hull.

USPEX. In the search for new crystal structures, it is practically impossible to sample all of the possible different configurations in which the atoms and the unit cell of a crystal can arrange, due to the large number of degrees of freedom present. Fortunately, not the entire space has to be sampled, but only some small regions around a known minimum. To achieve this, efficient methods are needed to explore these small regions.[29] In the search for new stable combinations of anhydrous $MgCl_2$ and $CaCl_2$, next to the manually doped structures, the evolutionary algorithm USPEX[29,31,45,46] was used in combination with its variable composition tool.[30,47] This is an efficient and proved evolutionary algorithm for crystal structures prediction, e.g., various ionic, covalent, metallic, and molecular structures.

USPEX uses random structures as well as combinations and perturbations of the most promising structures of previous generations to create a new generation of structures. From the new generation, the most promising structures will be selected, next to a set of randomly generated structures. The selection of most stable structures, in combination with good variation operators, allows one to zoom in on the most promising configurations, with the lowest amount of free energy, and converge to the most stable state. The randomly generated structures prevent one to be stuck around a single local minimum and explore other completely different solutions. The generated USPEX structures were relaxed using VASP with the same accuracy as the manually doped structures.

Convex Hull. To study the thermodynamical stability of the different combined salt hydrates, the convex hull was used. This provides insights into the stability of the individual doped structures, relative to the pure structures. The convex hull is the surface of the formation energy as a function of the chemical composition, which passes through all thermodynamically stable structures that are the lowest in energy. All structures, which are higher in energy, will be above this surface and can be considered as metastable structures. These metastable structures will possibly decompose, over (infinite) time, into a linear combination of the more stable structures located on the convex hull. The energy distance between the convex hull and any structure (dE_{CH}) gives us a measure for the (meta)stability of the structure.

To create the convex hull for each doped hydrate, we considered the original pristine crystals of $MgCl_2$,[32] $CaCl_2$,[32] $MgCl_2{\cdot}2H_2O$,[33] $CaCl_2{\cdot}2H_2O$,[34] $MgCl_2{\cdot}4\ H_2O$,[35] $CaCl_2{\cdot}4H_2O$,[36] $MgCl_2{\cdot}6H_2O$,[37] and $CaCl_2{\cdot}6H_2O$[38] as reference. The doped structures were compared to these reference structures by subtracting the reference energy multiplied by the fraction of the reference. An example of this calculation is given in Table 1. Furthermore, a ternary convex hull was created, combining the hydrates, using $MgCl_2$, $CaCl_2$, and the H_2O gas molecule as reference structures.

Chemical Bonding Analysis. The interatomic bonds of the most stable structures were qualified and quantified using the electron density-based methods, the Bader topological analysis, and the Density Derived Electronic and Chemical (DDEC6) approach.

Table 1. Example Calculation for the Convex Hull, Where the Energy Difference from the Convex Hull (E_{CH}) Can Be Computed by Subtracting the Reference Energy (E_{ref}) of the Pristine Systems from the Energy of the Compound Systems (E_{mix})

mixture		
salt A	salt B	energy difference with convex hull (E_{CH})
100%	0%	$E_{CH} = E_{mix} - 1 \times E_{ref,A} - 0 \times E_{ref,B} = 0$
95%	5%	$E_{CH} = E_{mix} - 0.95 \times E_{ref,A} - 0.05 \times E_{ref,B}$
90%	10%	$E_{CH} = E_{mix} - 0.9 \times E_{ref,A} - 0.1 \times E_{ref,B}$
...	...	
n	m	$E_{CH} = E_{mix} - n \times E_{ref,A} - m \times E_{ref,B}$
...	...	
0%	100%	$E_{CH} = E_{mix} - 0 \times E_{ref,A} - 1 \times E_{ref,B} = 0$

https://dx.doi.org/10.1021/acs.jpcc.0c05799
J. Phys. Chem. C 2020, 124, 24580−24591

For the characterization of the bond strength, we used the Density Derived Electronic and Chemical (DDEC6) method.[48−50] This method, which can provide reliable bond orders (BO) and net atomic charges (NAC), has been previously used to investigate the interactions and reactivity of various systems, e.g., molecular systems,[51,52] two-dimensional (2D) materials,[53] and porous media.[54]

To characterize the type of interactions (ionic, vdW, covalent, or a combination) between the atoms, the Quantum Theory of Atoms in Molecules (QTAIM) was used.[55−57] Within this framework, we investigated the topological analysis of the electron density, whereby the electron density characteristics at the bond critical points, as well as the values of the Laplacian, kinetic, and potential energy densities, can offer insight into both the strength and type of the interactions present[55−58] (see Table 2).

Table 2. Type of Interactions[58] Based on Bader Topological Analysis[a]

interaction	$\nabla^2\rho\ (r)$	$\lvert V\rvert/G$
covalent	<0	>2
transition	>0	1< ... < 2
ionic, vdW	>0	<1

[a] ρ is the electronic density, V is the potential energy density, and G is the kinetic energy density.

RESULTS AND DISCUSSION

Using evolutionary algorithms and electronic density-derived tools, the effect of doping magnesium chloride hydrates with calcium and vice versa is studied. The crystal stability (convex hull), the potential volumetric energy density (storage density), and the atomic interactions are quantified and qualified. Furthermore, trends in the effect of doping on the HCl interactions are explored

Convex Hull—Stability of the Explored Structures. New combinations of $MgCl_2{\cdot}nH_2O$ and $CaCl_2{\cdot}nH_2O$ (n = 0, 2, 4, 6) were explored using manually built configurations. In addition, the set of configurations for the anhydrous salt ($MgCl_2$, $CaCl_2$) was expanded using the evolutionary algorithm USPEX, to gain more knowledge on the possible combinations and structures. The use of USPEX for the di- and tetrahydrated salts was not feasible because of the high amount in degrees of freedom when four or more variable atoms/molecules are included.

The evolutionary algorithm USPEX search resulted in more than 3400 generated anhydrous structures, containing 18−36 atoms, over 25 generations. The known experimental structures of pure salts were used as seeds in the search, to enable a good start for a subset of the first generation. The convex hull of the most stable generated USPEX structures is shown in Figure 2a, with pure $MgCl_2$ on the left-hand side and pure $CaCl_2$ on the right-hand side of the x-axis. The energy is given per block of $MgCl_2/CaCl_2$. As shown in Figure 2a, all of the newly found structures with USPEX are above the dashed line. This line represents the convex hull and joins the most stable structures, in our case, the pure $MgCl_2$ and pure $CaCl_2$. This indicates that all found doped structures are metastable compared to the pure structures. This outcome agrees with the Aflow[28] database, which only contained the metastable combined structure $MgCaCl_4$ (represented with a red circle in Figure 2a), and does not report on any stable combination besides the pristine structures.

The results of the manually doped anhydrous and hydrated structures are given in Figure 2b, which also includes the most stable structures from USPEX. Similar structures were found; however, for the higher amount of doping ($\gtrsim$20%), USPEX found more stable structures than were found by manually doping the anhydrous structures. One can immediately see that all of the energies of the manual doped structures are also above the convex hull. Therefore, the convex hull turns out to be a straight surface between the pure salts. This indicates that all the generated combined structures are thermodynamically less stable than their pure compounds, and over (infinite) time, the metastable doped structures could decompose into the pure forms of $MgCl_2{\cdot}nH_2O$ and $CaCl_2{\cdot}nH_2O$. The metastable compounds could cause undesired reduced melting temperatures for the compound structures, which was already a problematic issue for the higher hydrates of $CaCl_2{\cdot}nH_2O$. However, the energy difference of the most stable doped structures for n = 0, 2, 4 (found along the dashed line in Figure 2b) with the convex hull is small (E_{CH} < 0.05 eV per block of $MgCl_2/CaCl_2/H_2O$), especially for low amounts of doping (<20%), compared with the inherent energy fluctuation in the order of 0.025 eV at room temperature. Therefore, we could assume that these generated doped structures are stable enough, and the energy difference is not large enough to let the doped structures decompose into grains of pure salts. For the hexahydrate (n = 6), one could conclude that, in general, doping increases instability more, compared to the lower hydrates, except for the case around 33% calcium content. In practice, this is also the case for pristine $CaCl_2{\cdot}6H_2O$, which is hardly studied as TCM material because it melts at room temperature.[7,12,13] The decreased stability implies that doping $CaCl_2{\cdot}6H_2O$ with magnesium does not prevent the undesired melting. The drop in E_{CH} for the hexahydrate structures with 33−66% calcium is caused by a distortion in the interaction plane parallel to the lattice c-direction, as shown in the Supporting Information. This leads to a stabilization of the crystal compared to the structures with a lower amount of calcium ($\lesssim$25%). The higher amount of calcium ($\gtrsim$75%) structures are structures corresponding to the $CaCl_2{\cdot}6H_2O$ topology.

Furthermore, we note that for a higher amount of doping, the anhydrous and dihydrate original structures of the undoped materials are no longer the preferred structures, but rather that of the dopant. Thus, for anhydrous structures, the combination of $Mg_xCa_{(1-x)}Cl_2$ (x > 44%) in $MgCl_2$ structure is less stable than the same combination but in the $CaCl_2$ structure, and vice versa $Mg_xCa_{(1-x)}Cl_2$ (x < 56%) in $CaCl_2$ structure is less stable than the same combination in $MgCl_2$ structure. For the dihydrate structures, this effect is also present, with the switch around 40%, however with a lower energy difference between the different structures. For the tetrahydrates, this effect is not observed. Thus, the preference of the crystal structure of the dopant becomes lower with an increasing amount of water in the crystal. Besides the hydration level, this effect could be also due to the fact that anhydrous $MgCl_2$ adopts a different crystal structure than $CaCl_2$ (rhombohedral vs orthorhombic crystal system). On the other hand, their corresponding hydrates crystallize in the orthorhombic and monoclinic crystal systems. The orthorhombic−monoclinic phase transition (in this case occurring for the hydrate variant) is more often reported in the

https://dx.doi.org/10.1021/acs.jpcc.0c05799
J. Phys. Chem. C 2020, 124, 24580−24591

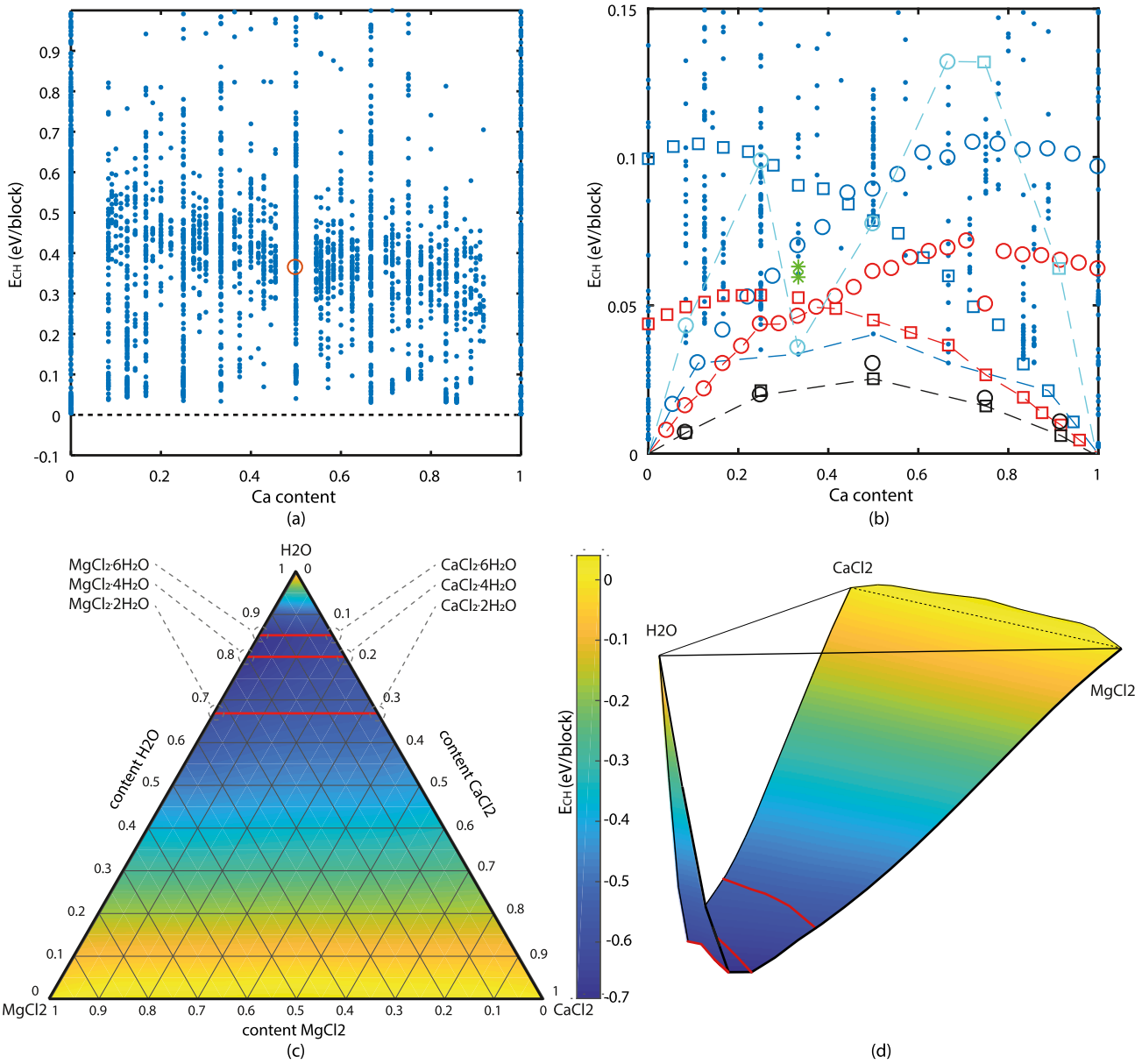

Figure 2. (a) USPEX convex hull for nonhydrated combinations of $MgCl_2$ and $CaCl_2$ (E < 1 eV/block). The energy is given per interchangeable block of $MgCl_2/CaCl_2$, thus per block of three atoms. The black dashed line represents the convex hull. The red circle indicates the metastable $MgCaCl_4$ structure given in the Aflow[28] database. (b) Convex hull of doped salt anhydrous and hydrated salts. The blue dots represent the most stable (E_{CH} < 0.15 eV/block) USPEX structures, the blue symbols represent the manually doped anhydrous structures (circle = doped $CaCl_2$; square = doped $MgCl_2$), the red symbols represent the dihydrate structures (circle = doped $CaCl_2{\cdot}4H_2O$; square = doped $CaCl_2{\cdot}2H_2O$), the black symbols represent the tetrahydrate structures (circle = doped $MgCl_2{\cdot}4\ H_2O$; square = doped $CaCl_2{\cdot}4H_2O$), and the cyan symbols represent the hexahydrate structures (circle = doped $MgCl_2{\cdot}6H_2O$; square = doped $CaCl_2{\cdot}6H_2O$). The convex hull energy is given in eV per block $MgCl_2$ or $CaCl_2$. The two green asterisks (*) are two experimentally found[34,59] and relaxed tachyhydrite structures ($CaMg_2Cl_6{\cdot}12H_2O$). The dashed lines connect the structures, which are further considered in this study. (c) Ternary figure of doped $MgCl_2{\cdot}nH_2O$ and $CaCl_2{\cdot}nH_2O$, with $MgCl_2$(s), $CaCl_2$(s), and H_2O(g) as reference structures. The energy is given in eV per block of ($MgCl_2/CaCl_2/H_2O$). The red lines highlight the di-, tetra-, and hexahydrate structures. (d) Three-dimensional (3D) visualization of the ternary convex hull.

literature than the orthorhombic−rhombohedral phase transition (in this case occurring for the anhydrous variant).

Interestingly, the experimental structures of tachyhydrite[59,60] ($CaMg_2Cl_6{\cdot}12H_2O$) are higher in energy than the generated doped structures. This could indicate that this is a metastable structure, or it is stabilized by entropy. The dashed lines (blue for anhydrous, red for dihydrates, black for tetrahydrates, and cyan for hexahydrates) in Figure 2b connect the most stable doped structures. These structures were used for further analysis in this study, including the obtained ternary convex hull, which is given in Figure 2c, and in a 3D image in Figure 2d. The 3D figure shows the relatively low energy difference with the convex hull of the doped structures within each hydrate, compared to the convex hull energy difference between doped structures of the different hydrates (ca. 0.6−0.7 eV). A close observation of Figure 2c,2d shows a heat of formation of 0.60, 0.69, 0.68, 0.54, 0.61, and 0.64 eV for $MgCl_2{\cdot}2H_2O$, $MgCl_2{\cdot}4\ H_2O$, $MgCl_2{\cdot}6\ H_2O$, $CaCl_2{\cdot}2H_2O$, $CaCl_2{\cdot}4H_2O$, and $CaCl_2{\cdot}6H_2O$ respectively, thus slightly higher values for the $MgCl_2$ hydrate reactions. The values

https://dx.doi.org/10.1021/acs.jpcc.0c05799
J. Phys. Chem. C 2020, 124, 24580−24591

are given per mol of $MgCl_2/CaCl_2/H_2O$ block, which equals heats of formation of 0.91, 0.87, 0.80, 0.81, 0.76, and 0.75 eV/mol of H_2O, respectively. The heat of formation per mol H_2O is in agreement with reference values of the NBS tables,[61] which are derived from measured reaction enthalpies and corrected to standard conditions. The comparison is given in Table 3.

Table 3. Heat of Formation for the Considered Reactions Compared with Calculated Values from NBS Tables[61]

	heat of formation		
phase transition	this work		NBS tables[61]
$MgCl_2{\cdot}nH_2O$	$(eV/(n_{MgCl_2}+n_{H_2O}))^a$	$(eV/n_{H_2O})^b$	$(eV/n_{H_2O})^c$
0–2	0.60	0.91	0.80
0–4	0.69	0.87	0.75
0–6	0.68	0.80	0.70
2–4		0.83	0.70
4–6		0.66	0.60
$CaCl_2{\cdot}nH_2O$	$(eV/(n_{CaCl_2}+n_{H_2O}))^a$		
0–2	0.54	0.81	0.65
0–4	0.61	0.76	0.64
0–6	0.64	0.75	0.65
2–4		0.71	0.63
4–6		0.73	0.69

[a]Energy given per mol of $MgCl_2/CaCl_2/H_2O$, as given in Figure 2c. [b]Energy given per mol H_2O. [c]Energy given per mol H_2O calculated from NBS tables[61] under standard conditions (T = 298 K, p = 1 bar).

Storage Density. The volumetric energy density of thermal energy storage is an important design parameter, and it is a unique selling point of TCM toward conventional thermal energy storage systems. In this sense, we computed the sorption energy of the different doped salts, to gain insight into the theoretical achievable energy density of the TCM storage. The sorption energy was computed using the most stable structures (connected by the dashed lines in Figure 2b) via

$$E_{\mathrm{sorp},x,m\to n} = E_{\mathrm{Mg}_{(1-x)}\mathrm{Ca}_x\mathrm{Cl}_2\cdot n\mathrm{H_2O}} - E_{\mathrm{Mg}_{(1-x)}\mathrm{Ca}_x\mathrm{Cl}_2\cdot m\mathrm{H_2O}} - (n-m)\times E_{\mathrm{H_2O}} \quad (1)$$

where $E_{\mathrm{sorp},x,m\to n}$ is the sorption energy between hydrates m and n at a given doping content x of calcium. $E_{Mg_{(1-x)}Ca_xCl_2\cdot nH_2O}$ is the crystal energy of the higher hydrate, $E_{Mg_{(1-x)}Ca_xCl_2\cdot mH_2O}$ is the crystal energy of the lower hydrate, and E_{H_2O} is the energy of water vapor. Accordingly, the volumetric energy density (E_{vol}) was computed using the volume (V_n) of the higher hydrated structure

$$E_{\mathrm{vol},x} = \frac{|E_{\mathrm{sorp},x,m\to n}|}{V_{n,x}} \quad (2)$$

As different amounts of doping (x) are present for the variable hydration numbers, an interpolation was used to generate the x-dependent variables from eqs 1 and 2. In Figure 3a, the results are given for the volumetric energy density. The asterisks (*) indicate calculated storage densities, using the formation energies of the NBS tables[61] divided by the volume of the experimental structures. The small discrepancy between these computed volumetric energy densities is mostly caused by the difference in formation energy.

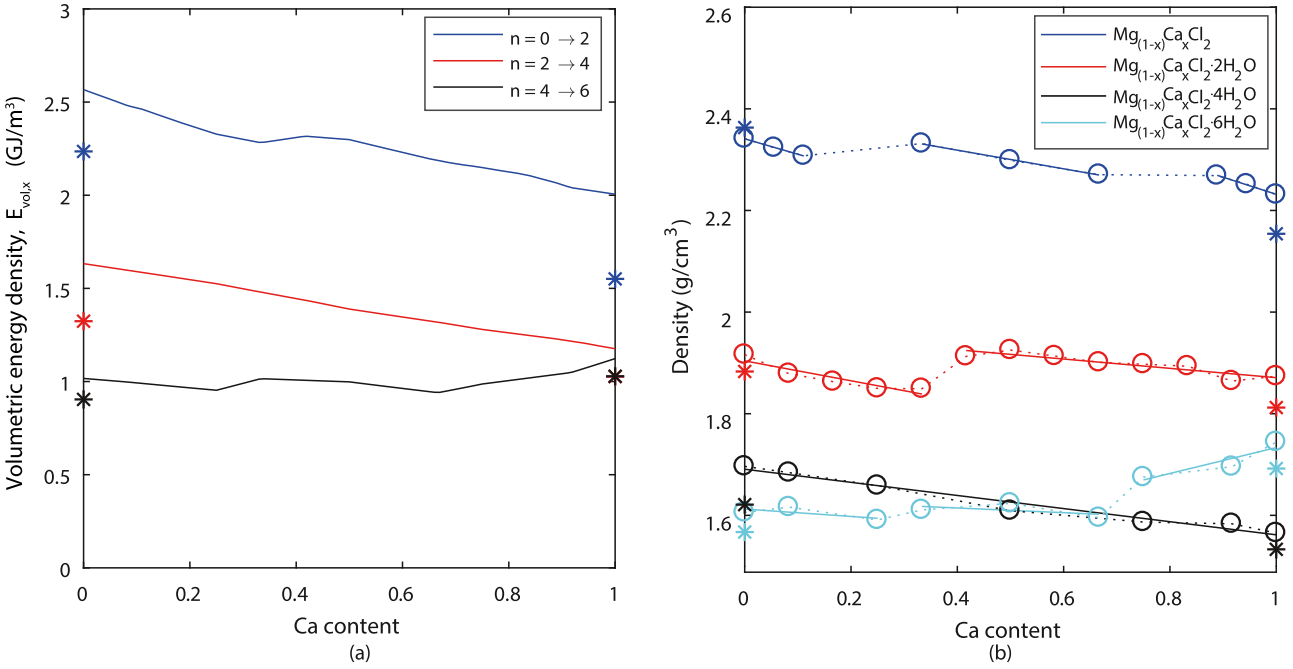

Figure 3. (a) Volumetric energy density of doped crystal structures. The red line represents the anhydrous to dihydrate (n = 0 → n = 2) reaction. The blue line represents the dihydrate to tetrahydrate (n = 2 → n = 4) reaction. The black line represents the tetrahydrate to hexahydrate (n = 4 → n = 6) reaction. The asterisks represent the calculated values using the NBS tables data.[61] (b) Density of doped salt hydrate crystals. Blue represents the anhydrous structures $Mg_{(1-x)}Ca_xCl_2$, red represents the dihydrate structures $Mg_{(1-x)}Ca_xCl_2{\cdot}2\ H_2O$, black represents the tetrahydrate structures $Mg_{(1-x)}Ca_xCl_2{\cdot}4\ H_2O$, and cyan represents the hexahydrate structures $Mg_{(1-x)}Ca_xCl_2{\cdot}6\ H_2O$, with x being the amount of Ca content. The dotted lines follow the most stable structures of the hydrates connected by the dashed lines in Figure 2b.

https://dx.doi.org/10.1021/acs.jpcc.0c05799
J. Phys. Chem. C 2020, 124, 24580−24591

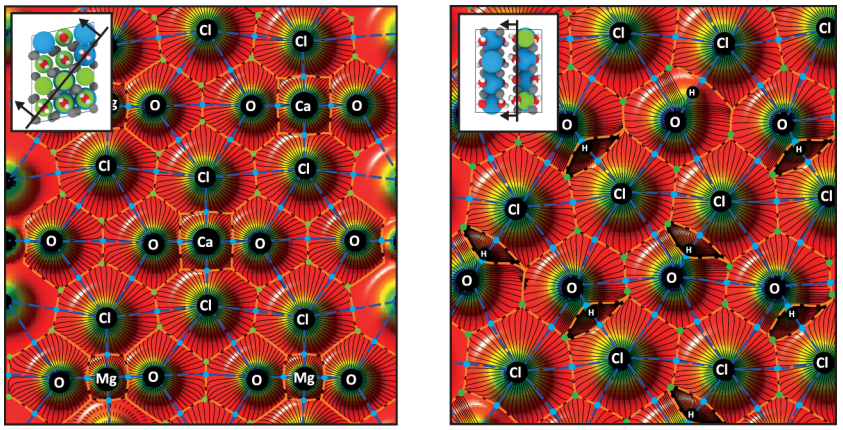

Figure 4. Topological analysis, with relevant section planes for (a) $Mg_{0.75}Ca_{0.25}Cl_2{\cdot}2\ H_2O$ and (b) $Ca_{0.75}Mg_{0.25}Cl_2{\cdot}2\ H_2O$.[18] The insets indicate the locations of the sections. The graphical colored background represents the electronic density in the plane. The superimposed lines allow for the topological analysis. The dashed blue lines designate bond paths, while the orange ones enclose the atomic basins. The blue dots designate the bond critical points (BCP), and the green dots indicate the ring critical points. The black lines are the gradient field lines.

The material densities of the different doped salt hydrates are given in Figure 3b. When considering the pristine structures (pure $MgCl_2{\cdot}nH_2O$ and pure $CaCl_2{\cdot}nH_2O$), the density difference between magnesium chloride and calcium chloride salts is −5, −2, −8, and 9% for anhydrous, dihydrate, tetrahydrate, and hexahydrate, respectively. However, when considering the trends of smaller separate sections of the anhydrous, dihydrate, and hexahydrate doped structures, the density decrease is relatively larger than the overall trend. These smaller sections are indicated by the solid lines in Figure 3b (the sections of 0−11, 33−66, and 89−100% calcium content for anhydrous structures; 0−33 and 42−100% calcium content for dihydrate structures; 0−25, 33−66, and 75−100% calcium content for hexahydrate structures). This effect is caused by a change in crystal structure and leads to extra voids, particularly for smaller amounts of doping. For example, anhydrous $MgCl_2$ already increases with 1.3% in volume when only 10% of calcium is added. Similarly, $MgCl_2{\cdot}2H_2O$ already increases with 1.0% in volume, and $MgCl_2{\cdot}6H_2O$ increases with 0.4% in volume when 10% of calcium is added. This is much larger than what the overall trends of the volume increase suggests, from which one would expect a volume increase of 0.5, 0.2, 0.8, and −9% when 10% of calcium is added to the magnesium structures. Thus, when small amounts of calcium are added to $MgCl_2{\cdot}nH_2O$, as long as it will remain in its original pristine crystal structure, the steric effect of the larger calcium atom will cause an even larger volume increase. Accordingly, near the crystal surface, these steric effects may promote valuable water dissociation and kinetics, as shown before in similar systems.[22,24] This effect of a relatively large volume increase is not present for the tetrahydrate structures, which can be linked to the fact that we did not observe a clear preferred crystal structure for this hydration level at different amounts of doping, but only small energy differences in the convex hull, as shown in Figure 2b.

Chemical Bonding Analysis. To study the interaction between atoms in doped crystals, the Bader Topological analysis, as well as DDEC6 methodology were used. Both methods are electronic density-based tools to qualify and quantify interactions between atoms. For this study, all of the doped crystals of the dihydrate form were used ($Ca_xMg_{(1-x)}Cl_2{\cdot}2H_2O$ and $Mg_{(1-x)}Ca_xCl_2{\cdot}2\ H_2O$, with x = [0, 1]). The dihydrate was chosen because HCl formation mainly happens when heating the lower (n = 1,2) hydrates;[11,16] and there are known experimental structures for both pure magnesium and calcium chloride dihydrate structures.

The Bader topological analysis builds upon the electronic density, and its Laplacian, at critical points within the crystal. An example of this analysis is given in Figure 4, where two relevant section planes are presented for $Mg_{0.75}Ca_{0.25}Cl_2{\cdot}2H_2O$ and $Ca_{0.75}Mg_{0.25}Cl_2{\cdot}2H_2O$. These section planes were chosen because they show the Ca/Mg−O, Ca/Mg−Cl, O−H, and H−Cl interactions. From these section planes, one can also see, e.g., the larger electronic radius of calcium compared to magnesium; the fact that hydrogen, although is closely—and thus strongly—bonded with oxygen, also shares a bond critical point (BCP) with chlorine.

At the BCP, the kinetic and potential energy densities were computed, From their combination (see Table 2), information on the type of the interactions can be obtained (reported in Table 4). Additionaly, in Table 4, we also report the DDEC6 bond orders (BO), which provides information on the amount of bonding electron pairs between atoms. From Table 4, one can see that O−H bonds are strongly covalent, while the H−Cl bonds are also covalent, albeit with a more significant polar character. The magnesium and calcium bonds are around the transition point but slightly more ionic than covalent. When adding calcium to the structure, the bond order in O−H increases, making this bond stronger and the water molecule more stable. Simultaneously, this bond becomes slightly less covalent. From Table 4, we also note that the Ca−Cl bonds have 17% stronger bonds (bond orders) than the Mg−Cl bonds. This further suggests that the presence of calcium in a structure will decrease its likelihood for HCl formation, compared with the presence of magnesium. The sum of bond order (SBO) is the summation of all BO per atom and provides information on how much the electron shells of the atoms are filled, and points to the reactivity of the atoms. The values of the SBOs from Table 5 indicate that the Ca atoms—following the formation of stronger bonds with Cl—have a higher SBO than Mg, and will be less reactive, accommodating less water molecules. This can be correlated to the experimental results where magnesium chloride can easily go

https://dx.doi.org/10.1021/acs.jpcc.0c05799
J. Phys. Chem. C 2020, 124, 24580−24591

Table 4. Chemical Bonding Analysis[18,a,b]

	x	$MgCl_2{\cdot}2H_2O$ crystal structure		$CaCl_2{\cdot}2H_2O$ crystal structure	
bond	% Ca	BO	$\frac{\lvert E_{pot}\rvert}{E_{kin}}$	BO	$\frac{\lvert E_{pot}\rvert}{E_{kin}}$
Mg−Cl	0	0.20 ± 0.019	0.86	0.18 ± 0.005	0.86
	25	0.19 ± 0.016	0.86	0.18 ± 0.010	0.86
	50	0.20 ± 0.014	0.86	0.18 ± 0.012	0.86
	75	0.20 ± 0.009	0.86	0.18 ± 0.011	0.85
	100				
Ca−Cl	0				
	25	0.24 ± 0.017	0.97	0.22 ± 0.011	0.96
	50	0.24 ± 0.018	0.97	0.21 ± 0.014	0.95
	75	0.24 ± 0.012	0.96	0.22 ± 0.012	0.95
	100	0.24 ± 0.011	0.96	0.22 ± 0.009	0.95
Mg−O	0	0.29 ± 0.000	0.88	0.28 ± 0.000	0.89
	25	0.28 ± 0.003	0.88	0.28 ± 0.003	0.89
	50	0.28 ± 0.005	0.88	0.28 ± 0.004	0.89
	75	0.27 ± 0.004	0.87	0.28 ± 0.003	0.89
	100				
Ca−O	0				
	25	0.29 ± 0.004	0.99	0.28 ± 0.004	0.98
	50	0.29 ± 0.006	0.99	0.28 ± 0.006	0.99
	75	0.28 ± 0.004	0.98	0.28 ± 0.004	0.98
	100	0.28 ± 0.000	0.97	0.28 ± 0.000	0.98
O−H	0	0.74 ± 0.000	7.12	0.74 ± 0.002	6.99
	25	0.75 ± 0.005	7.06	0.75 ± 0.005	6.86
	50	0.75 ± 0.006	6.96	0.75 ± 0.006	6.80
	75	0.76 ± 0.005	6.66	0.76 ± 0.006	6.73
	100	0.76 ± 0.001	6.84	0.76 ± 0.002	6.68
H−Cl	0	0.12 ± 0.000	1.15	0.12 ± 0.008	1.14
	25	0.12 ± 0.005	1.13	0.12 ± 0.023	1.15
	50	0.13 ± 0.006	1.14	0.12 ± 0.014	1.14
	75	0.13 ± 0.005	1.12	0.13 ± 0.011	1.14
	100	0.13 ± 0.001	1.12	0.13 ± 0.008	1.14

[a] $Mg_{(1-x)}Ca_xCl_2{\cdot}2\ H_2O$ starting from $MgCl_2{\cdot}2H_2O$, and $CaxMg_{(1-x)}Cl_2{\cdot}2H_2O$ starting from $CaCl_2{\cdot}2H_2O$, with x being the percentage of Ca [b] The bond order (BO) is computed within the DDEC6 approach. The potential energy density (E_{pot}) and the kinetic energy density (E_{kin}) are calculated within the QTAIM method at the bond critical points between the atoms, and the ratio is indicative of the type of the bond (see Table 2).

up to a higher level of hydrates, the higher hydrates melt at higher temperatures than hydrated calcium chloride crystals,[14] and the observed less stable $CaCl_2{\cdot}6H_2O$ related structures in the convex hull of Figure 2b.

Atomic Charges. DDEC6 net atomic charges for the dihydrate doped systems are given in Table 6. From this table, one can see that the average NAC remains similar for Mg, Ca, and Cl across different amounts of Mg and Ca. However, both the positive charge of H and the negative charge of O (both from H_2O) decrease gradually with the increase of Ca presence. A less polar water molecule will be less reactive and thus hinder the formation of the undesired HCl.

H−Cl Interactions. The Bader topological analysis and the DDEC6 method were performed on all of the generated dihydrate structures. This made it possible to investigate the H−Cl interaction within the structures and analyze possible trends. Accordingly, these trends could explain why $CaCl_2{\cdot}nH_2O$ is more resistant to hydrolysis than $MgCl_2{\cdot}nH_2O$. Furthermore, it could be used to study if doping could help $Mg_{(1-x)}Ca_xCl_2{\cdot}nH_2O$ to become more resistant to hydrolysis. In this section, we take a look at the trends in the H−Cl bond based on the chemical environment. In the previous paragraphs, it was already shown that chloride is stronger-bonded to calcium than magnesium, and the polarity of the water molecule decreases with higher amounts of calcium. In this section, we consider the H−Cl interaction within the different dihydrate crystals. To study this interaction, the local environment of the water molecule and chlorine atom, which are involved in the selected H−Cl interaction, was analyzed. More precisely, for a selected H−Cl bond, we investigated for the chlorine atom if it is (a) bonded to two Mg atoms, (b) bonded to one Mg and one Ca, or (c) bonded to two Ca atoms. Simultaneously, for the corresponding water molecule, we investigated if the oxygen atom was bonded to a magnesium or calcium atom. This approach is graphically depicted in Figure 5, and it provides insights into the effect of doping on the H−Cl interaction.

The difference in charge (Δq_{H-Cl}) between the hydrogen and chlorine atoms (from the respective H_2O and $Ca/MgCl_2$ molecules) versus their bond order is plotted in Figure 6a for all of the different kinds of environments an H−Cl bond can have. Relative to the highest charge difference in pristine $MgCl_2{\cdot}2H_2O$, the charge difference decreases on average with 0.7% when chlorine binds with one calcium atom, and with 1.6% if chlorine is bonded to two calcium atoms. Furthermore, the charge difference for these atoms will decrease further with an average of 0.7% if the oxygen atom bonds with calcium instead of magnesium. This results in a total drop 2.3% when moving from pristine $MgCl_2{\cdot}2H_2O$ to pristine $CaCl_2{\cdot}2H_2O$.

Simultaneously, relative to the pristine $MgCl_2{\cdot}2H_2O$ structure, the H−Cl bond order increases 2.8% if chlorine is bonded to two calcium atoms. In addition, the H−Cl bond

Table 5. Average Sum of Bond Orders (SBO) for the Doped Structures

system	%Mg	%Ca	Mg	Ca	Cl	O	H
$MgCl_2{\cdot}2H_2O$ + 0% Ca	100	0	1.39		1.15	2.13	0.92
$MgCl_2{\cdot}2H_2O$ + 25% Ca	75	25	1.37	1.62	1.11	2.10	0.93
$MgCl_2{\cdot}2H_2O$ + 50% Ca	50	50	1.39	1.61	1.12	2.08	0.93
$MgCl_2{\cdot}2H_2O$ + 75% Ca	25	75	1.37	1.57	1.09	2.07	0.94
$MgCl_2{\cdot}2H_2O$ + 100% Ca	0	100		1.59	1.06	2.04	0.94
$CaCl_2{\cdot}2H_2O$ + 100% Mg	100	0	1.33		1.16	2.15	0.93
$CaCl_2{\cdot}2H_2O$ + 75% Mg	75	25	1.33	1.51	1.15	2.13	0.94
$CaCl_2{\cdot}2H_2O$ + 50% Mg	50	50	1.32	1.48	1.12	2.11	0.94
$CaCl_2{\cdot}2H_2O$ + 25% Mg	25	75	1.32	1.50	1.10	2.09	0.95
$CaCl_2{\cdot}2H_2O$ + 0% Mg	0	100		1.50	1.08	2.07	0.95

https://dx.doi.org/10.1021/acs.jpcc.0c05799
J. Phys. Chem. C 2020, 124, 24580−24591

Table 6. Average Net Atomic Charges for Atoms in the Doped Crystal Structures[18]

System	%Mg	%Ca	Mg	Ca	Cl	O	H
$MgCl_2{\cdot}2H_2O$ + 0% Ca	100	0	1.340		−0.604	−0.870	0.402
$MgCl_2{\cdot}2H_2O$ + 25% Ca	75	25	1.343	1.295	−0.608	−0.857	0.400
$MgCl_2{\cdot}2H_2O$ + 50% Ca	50	50	1.337	1.301	−0.602	−0.849	0.395
$MgCl_2{\cdot}2H_2O$ + 75% Ca	25	75	1.342	1.314	−0.604	−0.839	0.391
$MgCl_2{\cdot}2H_2O$ + 100% Ca	0	100		1.305	−0.603	−0.827	0.389
$CaCl_2{\cdot}2H_2O$ + 100% Mg	100	0	1.361		−0.608	−0.868	0.394
$CaCl_2{\cdot}2H_2O$ + 75% Mg	75	25	1.362	1.339	−0.605	−0.860	0.394
$CaCl_2{\cdot}2H_2O$ + 50% Mg	50	50	1.362	1.347	−0.608	−-0.850	0.391
$CaCl_2{\cdot}2H_2O$ + 25% Mg	25	75	1.365	1.343	−0.605	−0.843	0.387
$CaCl_2{\cdot}2H_2O$ + 0% Mg	0	100		1.344	−0.605	−0.836	0.385

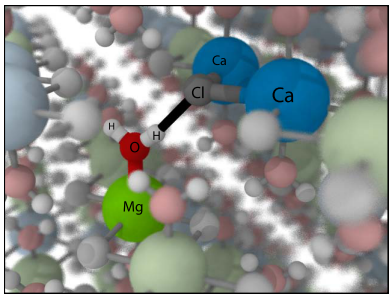

Figure 5. Visual representation of H−Cl interaction in Ca/Mg environment. The interaction is visualized as a black line.[18]

order will on average increase further with approximately 10% if the associated oxygen atom is bonded to calcium instead of magnesium. In the end, this results in a higher H−Cl bond order by 11.3% for pristine $CaCl_2{\cdot}2H_2O$ compared to pristine $MgCl_2{\cdot}2H_2O$. We observed before that chlorine has also a higher bond order with calcium than magnesium; thus, there is a positive correlation between the H−Cl bond order and the Cl−Mg/Ca bond order. Therefore, the chlorine atom will be harder to dissociate from a calcium atom than a magnesium atom, and the H−Cl bond is less likely to be formed in a calcium-rich environment despite its higher bond order. In this sense, we plotted in Figure 6b the H−Cl bond order divided by the Cl−Mg/Ca bond order. If we consider this "relative" bond order $\left(BO_{rel} = \frac{H - ClBO}{Ca/Mg - ClBO}\right)$, we see that, because both the H−Cl and Ca/Mg−Cl bond orders increase when going from a magnesium- to calcium-rich environment, the relative H−Cl bond order (BO_{rel}) does not increase. It actually even decreases slightly from an average relative bond order of $BO_{rel,H-Cl-MgMg}$ = 0.32 to $BO_{rel,H-Cl-CaCa}$ = 0.28 when comparing a chlorine atom that is two times bonded to a magnesium atom with a chlorine atom that is two times bonded to a calcium atom. In addition, the H−Cl charge difference decreases with a few percentages. The change is only

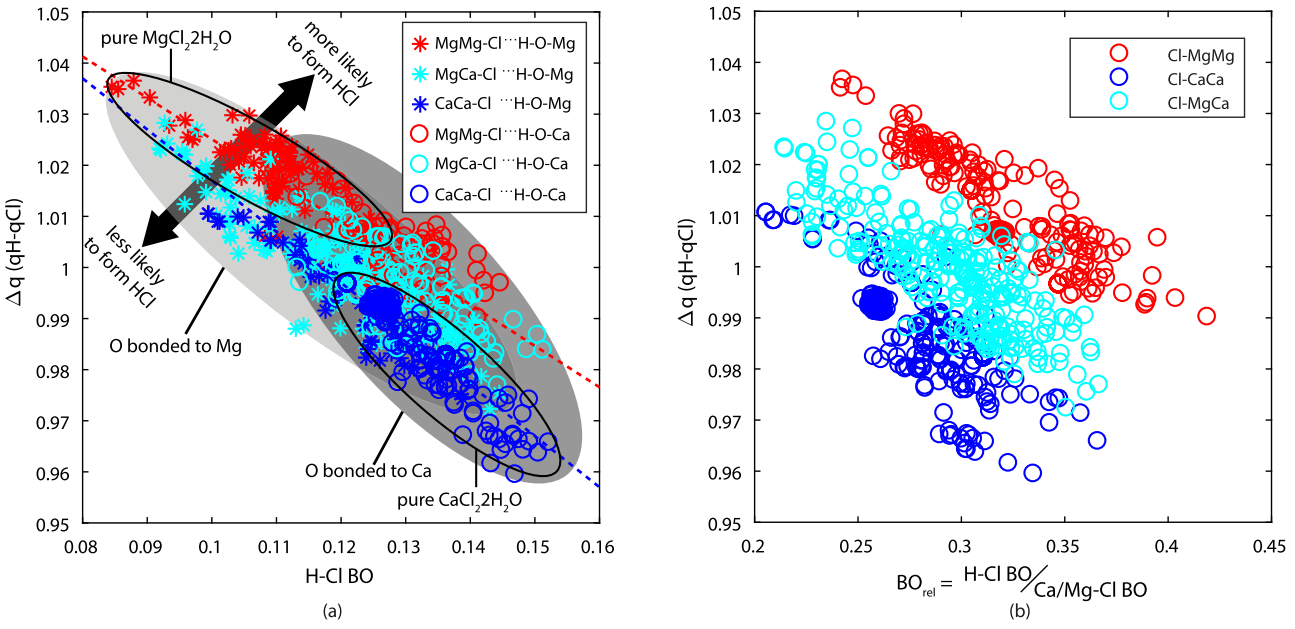

Figure 6. (a) Effect of calcium and magnesium environment on the interaction between the H and Cl atoms. The H−Cl bond order is given on the *x*-axis, and the charge difference between the H and Cl atom (Δq_{H-Cl}) is given on the *y*-axis. The asterisks (*) and circles (°) represent the different interactions of the oxygen atom with magnesium and calcium, respectively. The gray-shaded areas represent the differently bonded oxygen atoms. The different colors represent the different interactions of the chlorine atom. The red dashed line is a fit through the data where chlorine is bonded to two magnesium atoms, while the blue dashed line is a fit through the data where chlorine is bonded to two calcium atoms. The black circles represent the pure structures. (b) Effect of calcium and magnesium environment on the interaction between the H and Cl atoms. The H−Cl relative bond order (BO_{rel}) is given on the *x*-axis, and the charge difference between the H and Cl atom (Δq_{H-Cl}) is given on the *y*-axis.

https://dx.doi.org/10.1021/acs.jpcc.0c05799
J. Phys. Chem. C 2020, 124, 24580−24591

a few percentages; however, we know from experiments that pure magnesium chloride salt hydrates suffer from HCl formation, while this does not happen for calcium chloride salt hydrates within the application temperature window. Thereby, a small decrease in charge difference could be enough for excluding the H−Cl formation in thermal storage applications.

CONCLUSIONS

To improve low-temperature TCMs, extensive ab initio analysis was performed to investigate the impact of calcium doping on $MgCl_2{\cdot}nH_2O$ and that of magnesium doping on $CaCl_2{\cdot}nH_2O$. Manual doped anhydrous and hydrated $Mg_{(1-x)}Ca_xCl_2{\cdot}nH_2O$ structures were created by interchanging Mg and Ca atoms in known $MgCl_2{\cdot}nH_2O$ and $CaCl_2{\cdot}nH_2O$ structures. In addition, the evolutionary algorithm USPEX was used to explore new stable, anhydrous combinations of $MgCl_2$ and $CaCl_2$. The generated structures pointed out that the doped systems will be less stable than the pure salts. However, the energy difference between the metastable doped structures and the pure salts is small, thereby decompositions of the doped crystals into the more stable pure crystals will likely not occur. The hexahydrate structures were more affected by the doping than the lower hydrates. Nonetheless, a distortion in the $MgCl_2{\cdot}6H_2O$ crystals with calcium content above 25% resulted in a positive crystal stabilization.

The density was found to decrease, and volume was found to increase, with increasing the calcium content in the salts due to the larger calcium atom. Especially for low amounts of doping, when the crystal topology will not change, a significant volume increase occurs. Both the lower density and lower water sorption energy for calcium chloride systems lower the practically achievable energy storage density of the material. On the other hand, previous studies[22,24] showed that voids and defects, created by doping, could have an enhanced effect on the water dissociation, especially near the surface of the salt.

Chemical bonding analysis showed that a weaker interaction is present between Mg−Cl, compared to Ca−Cl. The combination of the weaker Mg−Cl interaction and the more polar H_2O molecule in magnesium chloride salt hydrates, compared to calcium chloride hydrates, gives rise to HCl formation. This is a highly undesired side reaction in magnesium chloride-based salts for heat storage.[11,16] Further analysis of the chemical environment of the H−Cl interaction showed that the presence of calcium atoms has a reducing effect on the H−Cl formation. This provided the possibility to shift the HCl formation outside the operational window of the thermochemical energy storage by doping magnesium chloride systems with calcium.

ASSOCIATED CONTENT

Supporting Information

The Supporting Information is available free of charge at https://pubs.acs.org/doi/10.1021/acs.jpcc.0c05799.

Crystal structure change of $MgCl_2{\cdot}6H_2O$ upon doping with calcium (PDF)

AUTHOR INFORMATION

Corresponding Authors

Ionut C. Tranca − *Department of Mechanical Engineering, Eindhoven University of Technology, Eindhoven 5600 MB, The Netherlands*; Email: i.tranca@tue.nl

Silvia V. Gaastra-Nedea − *Department of Mechanical Engineering, Eindhoven University of Technology, Eindhoven 5600 MB, The Netherlands*; Email: s.v.nedea@tue.nl

Authors

Koen Heijmans − *Department of Mechanical Engineering, Eindhoven University of Technology, Eindhoven 5600 MB, The Netherlands*; orcid.org/0000-0002-8940-935X

David M. J. Smeulders − *Department of Mechanical Engineering, Eindhoven University of Technology, Eindhoven 5600 MB, The Netherlands*

Complete contact information is available at: https://pubs.acs.org/10.1021/acs.jpcc.0c05799

Notes

The authors declare no competing financial interest.

ACKNOWLEDGMENTS

The authors thank the Netherlands Organization for Scientific Research (NWO) for access to the National High-Performance Computing Facility Cartesius, under project number #41921. This research received no external funding.

REFERENCES

(1) Fraunhofer et al. Mapping and Analysis of the Current and Future (2020-2030) Heating/Cooling Fuel Deployment (fossils/renewables), 2016. https://ec.europa.eu (accessed June 25, 2020).

(2) N'tsoukpoe, K. E.; Liu, H.; Le Pierrès, N.; Luo, L. A review on long-term sorption solar energy storage. *Renewable Sustainable Energy Rev.* **2009**, *13*, 2385−2396.

(3) Yu, N.; Wang, R.; Wang, L. Sorption thermal storage for solar energy. *Prog. Energy Combust. Sci.* **2013**, *39*, 489−514.

(4) Clark, R.-J.; Mehrabadi, A.; Farid, M. State of the art on salt hydrate thermochemical energy storage systems for use in building applications. *J. Energy Storage* **2020**, *27*, No. 101145.

(5) Scapino, L.; Zondag, H. A.; Van Bael, J.; Diriken, J.; Rindt, C. C. Sorption heat storage for long-term low-temperature applications: A review on the advancements at material and prototype scale. *Appl. Energy* **2017**, *190*, 920−948.

(6) Pardo, P.; Deydier, A.; Anxionnaz-Minvielle, Z.; Rougé, S.; Cabassud, M.; Cognet, P. A review on high temperature thermochemical heat energy storage. *Renewable Sustainable Energy Rev.* **2014**, *32*, 591−610.

(7) Donkers, P. A. J.; Sögütoglu, L. C.; Huinink, H. P.; Fischer, H. R.; Adan, O. C. G. A review of salt hydrates for seasonal heat storage in domestic applications. *Appl. Energy* **2017**, *199*, 45−68.

(8) Zhang, Y.; Wang, R. Sorption thermal energy storage: Concept, process, applications and perspectives. *Energy Storage Mater.* **2020**, *27*, 352−369.

(9) Zhang, Y.; Dong, H.; Wang, R.; Feng, P. Air humidity assisted sorption thermal battery governed by reaction wave model. *Energy Storage Mater.* **2020**, *27*, 9−16.

(10) Pathak, A. D.; Nedea, S.; Van Duin, A. C. T.; Zondag, H. A.; Rindt, C. C. M.; Smeulders, D. M. J. Reactive force field development for magnesium chloride hydrates and its application for seasonal heat storage. *Phys. Chem. Chem. Phys.* **2016**, *18*, 15838−15847.

(11) Zondag, H. A.; Van Essen, V. M.; Bleijendaal, L. P. J.; Kikkert, B. W. J.; Bakker, M. In *Application of MgCl2·6H2O for Thermochemical Seasonal Solar Heat Storage*, 5th International Renewable Energy Storage Conference (IRES 2010), Berlin, Germany, Nov 22−24, 2010.

(12) Ferchaud, C. J.; Zondag, H. A.; Veldhuis, J. B. J.; De Boer, R. Study of the reversible water vapour sorption process of MgSO4. 7H2O and MgCl2. 6H2O under the conditions of seasonal solar heat storage. *J. Phys.: Conf. Ser.* **2012**, *395*, No. 012069.

(13) Van Essen, V.; Cot Gores, J.; Bleijendaal, L.; Zondag, H.; Schuitema, R.; Bakker, M.; Van Helden, W. In *Characterization of Salt Hydrates for Compact Seasonal Thermochemical Storage*, ASME 2009 3rd International Conference on Energy Sustainability Collocated with the Heat Transfer and InterPACK09 Conferences, San Francisco, USA, July 19-23, 2009; pp 825−830.
(14) Haynes, W. M. *CRC Handbook of Chemistry and Physics*; CRC Press, 2014.
(15) Carlsson, B.; Stymne, H.; Wettermark, G. An incongruent heat-of-fusion system CaCl2 · 6H2O - Made congruent through modification of the chemical composition of the system. *Sol. Energy* **1979**, *23*, 343−350.
(16) Kipouros, G. J.; Sadoway, D. R. A thermochemical analysis of the production of anhydrous MgCl2. *J. Light Met.* **2001**, *1*, 111−117.
(17) Pathak, A. D.; Nedea, S.; Zondag, H.; Rindt, C.; Smeulders, D. A DFT-based comparative equilibrium study of thermal dehydration and hydrolysis of CaCl2 hydrates and MgCl2 hydrates for seasonal heat storage. *Phys. Chem. Chem. Phys.* **2016**, *18*, 10059−10069.
(18) Heijmans, K.; Tranca, I.; Nedea, S.; Smeulders, D. In *Ab-initio Study of Doped Salt Hydrates Crystal Stabilities for Thermochemical Heat Storage*, Advances in Thermal Energy Storage, Eurotherm Seminar #112, Lleida, Spain, May 15−17, 2019; pp 123−131.
(19) Rammelberg, H. U.; Myrau, M.; Schmidt, T.; Ruck, W. An Optimization of Salt Hydrates for Thermochemical Heat Storage. In *Touka Shobo (Hg.): Innovative Materials for Processes in Energy Systems*; Saha, B. B.; Saha, B. B.; Koyama, M.; Takata, Y.; Hamamoto, Y.; Miyazaki, T.; Masamichi, K.; Ito, K., Eds.; Impres, 2013; pp 550−555.
(20) Rammelberg, H. U.; Osterland, T.; Priehs, B.; Opel, O.; Ruck, W. K. Thermochemical heat storage materials-Performance of mixed salt hydrates. *Sol. Energy* **2016**, *136*, 571−589.
(21) Pathak, A. D.; Tranca, I.; Nedea, S. V.; Zondag, H. A.; Rindt, C. C.; Smeulders, D. M. First-Principles Study of Chemical Mixtures of CaCl2 and MgCl2 Hydrates for Optimized Seasonal Heat Storage. *J. Phys. Chem. C* **2017**, *121*, 20576−20590.
(22) Müller, D.; Knoll, C.; Ruh, T.; Artner, W.; Welch, J. M.; Peterlik, H.; Eitenberger, E.; Friedbacher, G.; Harasek, M.; Blaha, P.; et al. Calcium doping facilitates water dissociation in magnesium oxide. *Adv. Sustainable Syst.* **2018**, *2*, No. 1700096.
(23) Huinink, H. P.; Sansotta, S.; Zahn, D. Defect-driven water migration in MgCl2 tetra-and hexahydrates. *J. Solid State Chem.* **2019**, *277*, 221−228.
(24) Pathak, A. D.; Nedea, S.; Zondag, H.; Rindt, C.; Smeulders, D. Diffusive transport of water in magnesium chloride dihydrate under various external conditions for long term heat storage: A ReaxFF-MD study. *Eur. J. Mech., B: Fluids* **2017**, *64*, 93−101.
(25) Pathak, A. D.; Heijmans, K.; Nedea, S.; van Duin, A. C.; Zondag, H.; Rindt, C.; Smeulders, D. Mass diffusivity and thermal conductivity estimation of chloride-based salt hydrates for thermochemical heat storage: A molecular dynamics study using the reactive force field. *Int. J. Heat Mass Transfer* **2020**, *149*, No. 119090.
(26) Hu, X. L.; Carrasco, J.; Klimeš, J.; Michaelides, A. Trends in water monomer adsorption and dissociation on flat insulating surfaces. *Phys. Chem. Chem. Phys.* **2011**, *13*, 12447−12453.
(27) Abhat, A.; Huy, T. Heat and mass transfer considerations in a thermochemicalenergy storage system based on solid-gas reactions. *Sol. Energy* **1983**, *30*, 93−98.
(28) Oses, C.; Gossett, E.; Hicks, D.; Rose, F.; Mehl, M. J.; Perim, E.; Takeuchi, I.; Sanvito, S.; Scheffler, M.; Lederer, Y.; et al. AFLOW-CHULL: cloud-oriented platform for autonomous phase stability analysis. *J. Chem. Inf. Model.* **2018**, *58*, 2477−2490.
(29) Oganov, A. R.; Glass, C. W. Crystal structure prediction using ab initio evolutionary techniques: Principles and applications. *J. Chem. Phys.* **2006**, *124*, No. 244704.
(30) Oganov, A. R.; Ma, Y.; Lyakhov, A. O.; Valle, M.; Gatti, C. Evolutionary crystal structure prediction as a method for the discovery of minerals and materials. *Rev. Mineral. Geochem.* **2010**, *71*, 271−298.
(31) Lyakhov, A. O.; Oganov, A. R.; Stokes, H. T.; Zhu, Q. New developments in evolutionary structure prediction algorithm USPEX. *Comput. Phys. Commun.* **2013**, *184*, 1172−1182.
(32) Wyckoff, R. W. G. *Crystal Structures*; Interscience Publishers, 1963; Vol. 2, pp 239−444.
(33) Kaduk, J. A. Use of the inorganic crystal structure database as a problem solving tool. *Acta Crystallogr., Sect. B: Struct. Sci.* **2002**, *58*, 370−379.
(34) Leclaire, A.; Borel, M. Le dichlorure de calcium dihydraté. *Acta Crystallogr., Sect. B: Struct. Crystallogr. Cryst. Chem.* **1977**, *33*, 1608−1610.
(35) Schmidt, H.; Hennings, E.; Voigt, W. Magnesium chloride tetrahydrate, MgCl2·4H2O. *Acta Crystallogr., Sect. C: Cryst. Struct. Commun.* **2012**, *68*, i4−i6.
(36) Leclaire, A.; Borel, M.; Monier, J. La forme γ du dichlorure de calcium tétrahydraté. *Acta Crystallogr., Sect. B: Struct. Crystallogr. Cryst. Chem.* **1980**, *36*, 2757−2759.
(37) Agron, P.; Busing, W. Magnesium dichloride hexahydrate, MgCl2. 6H2O, by neutron diffraction. *Acta Crystallogr., Sect. C: Cryst. Struct. Commun.* **1985**, *41*, 8−10.
(38) Leclaire, A.; Borel, M. Le dichlorure et le dibromure de calcium hexahydrates. *Acta Crystallogr., Sect. B: Struct. Crystallogr. Cryst. Chem.* **1977**, *33*, 2938−2940.
(39) Kresse, G.; Furthmüller, J. Efficient iterative schemes for ab initio total-energy calculations using a plane-wave basis set. *Phys. Rev. B* **1996**, *54*, No. 11169.
(40) Perdew, J. P.; Burke, K.; Ernzerhof, M. Generalized gradient approximation made simple. *Phys. Rev. Lett.* **1996**, *77*, 3865.
(41) Blöchl, P. E. Projector augmented-wave method. *Phys. Rev. B* **1994**, *50*, 17953.
(42) Kresse, G.; Joubert, D. From ultrasoft pseudopotentials to the projector augmented-wave method. *Phys. Rev. B* **1999**, *59*, 1758.
(43) Grimme, S.; Antony, J.; Ehrlich, S.; Krieg, H. A consistent and accurate ab initio parametrization of density functional dispersion correction (DFT-D) for the 94 elements H-Pu. *J. Chem. Phys.* **2010**, *132*, No. 154104.
(44) Grimme, S.; Ehrlich, S.; Goerigk, L. Effect of the damping function in dispersion corrected density functional theory. *J. Comput. Chem.* **2011**, *32*, 1456−1465.
(45) Oganov, A. R.; Lyakhov, A. O.; Valle, M. How Evolutionary Crystal Structure Prediction Works and Why. *Acc. Chem. Res.* **2011**, *44*, 227−237.
(46) Bushlanov, P. V.; Blatov, V. A.; Oganov, A. R. Topology-based crystal structure generator. *Comput. Phys. Commun.* **2019**, *236*, 1−7.
(47) Lyakhov, A. O.; Oganov, A. R.; Valle, M. Crystal structure prediction using evolutionary approach. *Mod. Methods Cryst. Struct. Predict.* **2010**, 147−180.
(48) Manz, T. A.; Limas, N. G. Introducing DDEC6 atomic population analysis: part 1. Charge partitioning theory and methodology. *RSC Adv.* **2016**, *6*, 47771−47801.
(49) Limas, N. G.; Manz, T. A. Introducing DDEC6 atomic population analysis: part 2. Computed results for a wide range of periodic and nonperiodic materials. *RSC Adv.* **2016**, *6*, 45727−45747.
(50) Manz, T. A. Introducing DDEC6 atomic population analysis: part 3. Comprehensive method to compute bond orders. *RSC Adv.* **2017**, *7*, 45552−45581.
(51) Chen, T.; Manz, T. A. Bond orders of the diatomic molecules. *RSC Adv.* **2019**, *9*, 17072−17092.
(52) Rohling, R. Y.; Tranca, I. C.; Hensen, E. J.; Pidko, E. A. Correlations between density-based bond orders and orbital-based bond energies for chemical bonding analysis. *J. Phys. Chem. C* **2019**, *123*, 2843−2854.
(53) Man, I.-C.; Trancă, I.; Soriga, S.-G. First principle studies of oxygen reduction reaction on N doped graphene: Impact of N concentration, position and co-adsorbate effect. *Appl. Surf. Sci.* **2020**, *510*, No. 145470.
(54) Rohling, R. Y.; Tranca, I. C.; Hensen, E. J.; Pidko, E. A. Electronic Structure Analysis of the Diels−Alder Cycloaddition

https://dx.doi.org/10.1021/acs.jpcc.0c05799
J. Phys. Chem. C 2020, 124, 24580−24591

Catalyzed by Alkali-Exchanged Faujasites. *J. Phys. Chem. C* **2018**, *122*, 14733−14743.
(55) Bader, R. F. W. *Atoms in Molecules: A Quantum Theory*; Oxford University Press, 1998.
(56) Vega, D.; Almeida, D. AIM-UC: An application for QTAIM analysis. *J. Comput. Methods Sci. Eng.* **2014**, *14*, 131−136.
(57) Spackman, M. A. The Quantum Theory of Atoms in Molecules: From Solid State to DNA and Drug Design. *Angew. Chem., Int. Ed.* **2007**, *46*, 6766−6767.
(58) Cremer, D.; Kraka, E. Chemical bonds without bonding electron density - does the difference electron-density analysis suffice for a description of the chemical bond. *Angew. Chem., Int. Ed.* **1984**, *23*, 627−628.
(59) Clark, J. R.; Evans, H. T.; Erd, R. C. Tachyhydrite, dimagnesium calcium chloride 12-hydrate. *Acta Crystallogr., Sect. B: Struct. Crystallogr. Cryst. Chem.* **1980**, *36*, 2736−2739.
(60) Leclaire, A.; Borel, M. M.; Monier, J. C. Structure de la tachydrite. *Acta Crystallogr., Sect. B: Struct. Crystallogr. Cryst. Chem.* **1980**, *36*, 2734−2735.
(61) Wagman, D. D.; Evans, W. H.; Parker, V. B.; Schumm, R. H.; Halow, I.; Bailey, S. M.; Churney, K. L.; Nuttall, R. L. The NBS tables of chemical thermodynamic properties: Selected values for inorganic and C1 and C2 organic substances in SI units. *J. Phys. Chem. Ref. Data* **1989**, *18*, 1807−1812.

https://dx.doi.org/10.1021/acs.jpcc.0c05799
J. Phys. Chem. C 2020, 124, 24580−24591